Research Square

Preprints are preliminary reports that have not undergone peer review.
They should not be considered conclusive, used to inform clinical practice,
or referenced by the media as validated information.

Synthesis, DFT study, molecular docking and antibacterial evaluation of a nitrophenyl-thienochromenone azo ligand and its Mn(II), Co(II) and Fe(II) complexes

Emmanuel Sopbué Fondjo
sopbue@yahoo.fr

University of Dschang
Victor Bertold Atedjong Tedjong
University of Dschang
Jean-de-Dieu Tamokou
University of Dschang
Steve Perin Dadem Kemgou
University of Dschang
Sorelle Songmi Feuze
University of Dschang
André Désiré Siéwé
University of Dschang
Apollinaire Tsopmo
Carleton University
Peter Friedrich Wilhelm Simon
Rhine-Waal University of Applied Sciences
Bruno Ndjakou Lenta
Higher Teacher's Training College
Jules-Roger Kuiate
University of Dschang

Research Article

Keywords: Azo dye, thienochromenone, manganese complex, cobalt complex, iron complex, DFT, molecular docking, DNA gyrase, antibacterial activity

Posted Date: November 9th, 2026

DOI: https://doi.org/10.21203/rs.3.rs-11234575/v1

License: This work is licensed under a Creative Commons Attribution 4.0 International License.
Read Full License

Additional Declarations: No competing interests reported.

Synthesis, DFT study, molecular docking and antibacterial evaluation of a nitrophenyl-thienochromenone azo ligand and its Mn(II), Co(II) and Fe(II) complexes

Emmanuel Sopbué Fondjo*[a], Victor Bertold Atedjong Tedjong[a], Jean-de-Dieu Tamokou[b], Steve Perin. Dadem Kemgou[a], Sorelle Songmi Feuze[a], André Désiré Siéwé[a], Apollinaire Tsopmo[c], Peter Friedrich Wilhelm Simon[d], Bruno Lenta Ndjakou[e] and Jules Roger Kuiate[b]

[a]*Research Unit of Applied and Environmental Chemistry (RUAPEC), Department of Chemistry, Faculty of Science, University of Dschang, P.O. Box 067 Dschang, Republic of Cameroon*
[b]*Research Unit of Microbiology and Antimicrobial Substances, Department of Biochemistry, Faculty of Science, University of Dschang, PO Box 067 Dschang, Republic of Cameroon*
[c]*Department of Chemistry, Carleton University, 1125 Colonel By Drive K1S 5B6, Ottawa, Canada +1-613-520-260 Ext 3122*
[d]*Polymer Chemistry Laboratory, Faculty of Live Sciences, Rhine-Waal University of Applied Sciences, Campus Kleve, Marie-Curie Strasse 1, D-47533 Kleve, Germany*
[e]*Higher Teacher's Training College, University of Yaounde I; P. O. Box 47, Yaounde, Cameroon*.

✉Emmanuel Sopbué Fondjo; sopbue@yahoo.fr (https://orcid.org/0000-0002-1077-673X)
Victor Bertold Atedjong Tedjong: victorbertold@gmail.com (https://orcid.org/0009-0001-2201-9955)
Jean-de-Dieu Tamokou: jtamokou@yahoo.fr (https://orcid.org/0000-0002-8088-463X)
Steve Perin. Dadem Kemgou: dademsteve@gmail.com (https://orcid.org/0009-0002-8328-4936)
Songmi Feuze Sorelle: sorelsongmi@gmail.com (https://orcid.org/0009-0003-2223-0413)
André Désiré Siéwé: andredesiresiewe@yahoo.com (https://orcid.org/0000-0001-9686-4396)
Apollinaire Tsopmo:apollinaire.tsopmo@carleton.ca (https://orcid.org/0000-0002-7062-0833)
Peter F. W Simon: peter.simon@hochschule-rhein-waal.de (https://orcid.org/0000-0002-0297-8331)
Bruno Ndjakou Lenta: lentabruno@yahoo.fr (https://orcid.org/0000-0001-9095-6660)
Jules-Roger Kuiate: jrkuiate@yahoo.com (https://orcid.org/0000-0002-5134-9427)

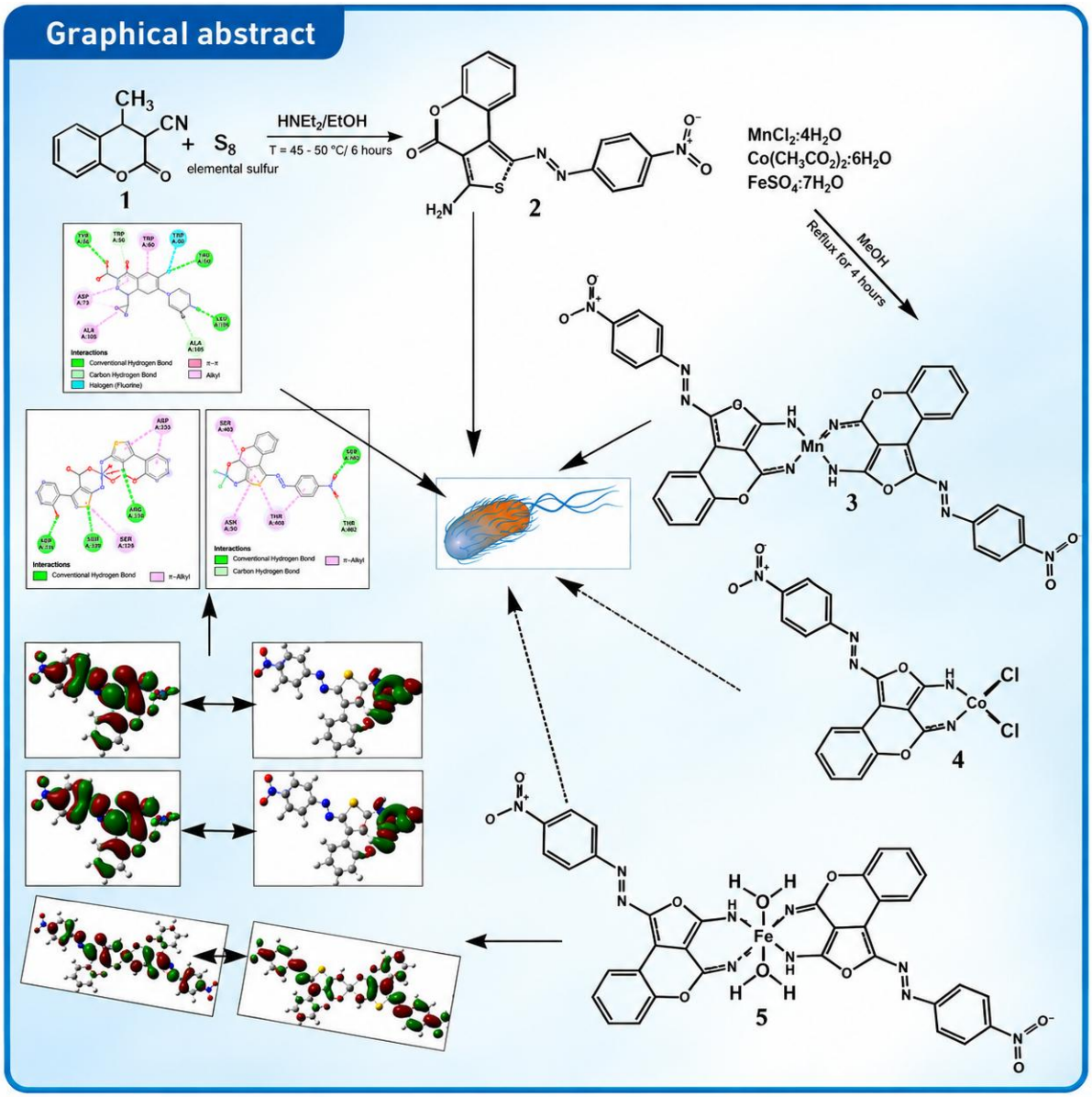
"Corresponding author: Prof. Dr. Emmanuel Sopbué Fondjo. E-mail: sopbue@yahoo.fr"

Abstract

The nitrophenyl-substituted azo-thienochromenone ligand 3-amino-1-[(E)-(4-nitrophenyl)diazenyl]-4*H*-thieno[3,4-c]chromen-4-one (**2**), obtained by diazo coupling on 3-amino-4*H*-thieno[3,4-c]chromen-4-one prepared via a modified Gewald cyclisation, was reacted with $MnCl_2 \cdot 4H_2O$, $CoCl_2 \cdot 6H_2O$ and $FeSO_4 \cdot 7H_2O$ to give three new complexes, **3** (Mn), **4** (Co) and **5** (Fe), characterised by HRESI-MS, UV-Vis, FT-IR, multinuclear/2D NMR and powder X-ray diffraction (PXRD), which

together established bidentate coordination of the ligand through the lactone carbonyl oxygen and the deprotonated aromatic amine nitrogen, leaving the azo bridge and nitro group uncoordinated. DFT calculations (B3LYP/6-311++G(d,p)) showed the HOMO-LUMO gap narrowing on complexation in the order **4** (1.679 eV) < **5** (2.085 eV) < **3** (2.513 eV) < **2** (2.737 eV), with **4** showing the highest electrophilicity index (ω = 16.143 eV). Molecular docking against E. coli DNA gyrase (7AB4), S. aureus DNA gyrase (1MWT) and P. aeruginosa lectin LecB (4NG2) ranked **3** as the most promising candidate, outperforming ciprofloxacin on 7AB4 and 1MWT, and broth microdilution confirmed this trend, with **3** giving the lowest MICs of the series (16 µg/mL against E. coli and S. aureus) while **5** was the only bactericidal compound against P. aeruginosa (MBC/MIC = 1). Overall, complexation of **2** with Mn(II), Co(II) and Fe(II) consistently enhanced antibacterial activity relative to the free ligand, with the manganese complex **3** standing out as the most active and computationally consistent candidate, supporting azo-thienochromenone metal complexes as a viable platform for antibacterial drug development.

Keywords: Azo dye; thienochromenone; manganese complex; cobalt complex; iron complex; DFT; molecular docking; DNA gyrase; antibacterial activity



Introduction

The continuing rise of antimicrobial resistance among clinically relevant Gram-positive and Gram-negative bacterial pathogens has renewed interest in metal-based antibacterial agents as an alternative, or complement, to conventional antibiotics [1,2]. Coordination compounds act through mechanisms distinct from those of classical organic antibiotics. Due to their ability to induce membrane disruption, redox generation of reactive oxygen species, and interference with bacterial DNA-replication enzymes they are less susceptible to the efflux-pump and target-mutation mechanisms underlying resistance to many organic drugs [3].

Azo compounds, characterised by the -N=N- chromophore, are recognised as versatile ligands in coordination chemistry owing to the additional donor atoms (N, O) usually located close to the azo bridge [4]. Combined with a coumarin fragment itself a privileged scaffold in medicinal chemistry on account of documented antibacterial, antioxidant and anticoagulant properties [5] azo-coumarin hybrids constitute an attractive platform for the design of new bioactive ligands. Thienochromenones, represent a group of bicyclic systems formed by fusion of a thiophene ring onto the coumarin core may be synthesized by a modified Gewald reaction. Previously been shown to give access, once diazotised and coupled to phenolic or amino partners the compound class has, to azo dyes with antibacterial and antifungal activity [6,7].

Recent work from our research group and from related teams has shown that complexation of such azo-thienochromenone ligands with first-row transition metals, notably Co(II) and Mg(II), enhances antibacterial potency relative to the free ligand, in agreement with Tweedy's chelation theory, according to which metal coordination lowers the polarity of the metal ion and favours penetration across the bacterial membrane [8-10]. Fondjo *et al*. have recently reported two Co(II) complexes of a structurally related azo-thienochromenone ligand, active against *Staphylococcus aureus* and *Escherichia coli* [9].

The present study concerns a new nitrophenyl-substituted azo-thienochromenone ligand, compound **2** 3-amino-1-[(E)-(4-nitrophenyl)diazenyl]-4*H*-thieno[3,4-c]chromen-4-one obtained by diazo coupling of 4-nitroaniline onto a 2-aminothiophene-thienochromenone precursor, together with its complexation by three divalent metal ions of biological relevance: Mn(II), Co(II) and Fe(II). The aminothienochromenone precursor 3-amino-4*H*-thieno[3,4-c]chromen-4-one was prepared following a modified Gewald route already established and validated by our group for this class of scaffold [6,7]. The nitrophenyl-coupled product itself corresponds structurally to a disperse azo dye previously reported by Al-Mousawi and El-Apasery for the dyeing of polyester fabric [11]; to best of our knowledge, the present work is the first to examine this compound as a coordinating ligand, and reports its complexation chemistry, DFT reactivity profile, molecular-docking behaviour and antibacterial activity. The choice of a nitro-substituted coupling partner was motivated by the

intention to build a push-pull electronic architecture, with the coumarin-thiophene-azo system acting as the electron donor and the nitrophenyl ring as the acceptor an arrangement also exploited in coumarin-based azo dyes described by Ayare et al. for their multifunctional properties [22]. The ligand and its three complexes were fully characterised by spectroscopic and computational methods, and their antibacterial potential was evaluated through a combined in silico/in vitro approach against three reference bacterial strains and their corresponding therapeutic targets.

Results and discussion

Chemistry

Synthesis and structural characterisation of ligand and complexes

The 3-amino-4*H*-thieno[3,4-c]chromen-4-one precursor **10** was obtained in two steps from 1-(2-hydroxyphenyl)ethan-1-one (2′-hydroxyacetophenone), by Knoevenagel condensation with ethyl 2-cyanoacetate (65.9%), followed by a Gewald-type cyclisation in the presence of elemental sulfur and diethylamine (93%). This protocol reproduces, without substantial modification, the synthetic route previously described and validated by our laboratory for access to 3-amino-4*H*-thieno[3,4-c]chromen-4-one derivatives [6,7], and the yields obtained here are consistent with those reported in that earlier work. The compound **2** ligand was then obtained by diazotisation of 4-nitroaniline in H_2SO_4/DMSO at 0–5 °C, followed by coupling with **10** and neutralisation with sodium acetate, giving a brown solid (Rf = 0.6, hexane/ethyl acetate 50:50). The synthetic route leading to ligand 2 is summarised in Fig. 1. It should be noted, for the sake of proper attribution, that the nitrophenyl-substituted product obtained through this route is structurally identical to a disperse azo dye reported by Al-Mousawi and El-Apasery in their study of arylazothienochromene dyes for polyester dyeing [11].

The synthetic route used for the preparation of coordination compounds 3, 4 and 5 is summarised in Fig. 2.

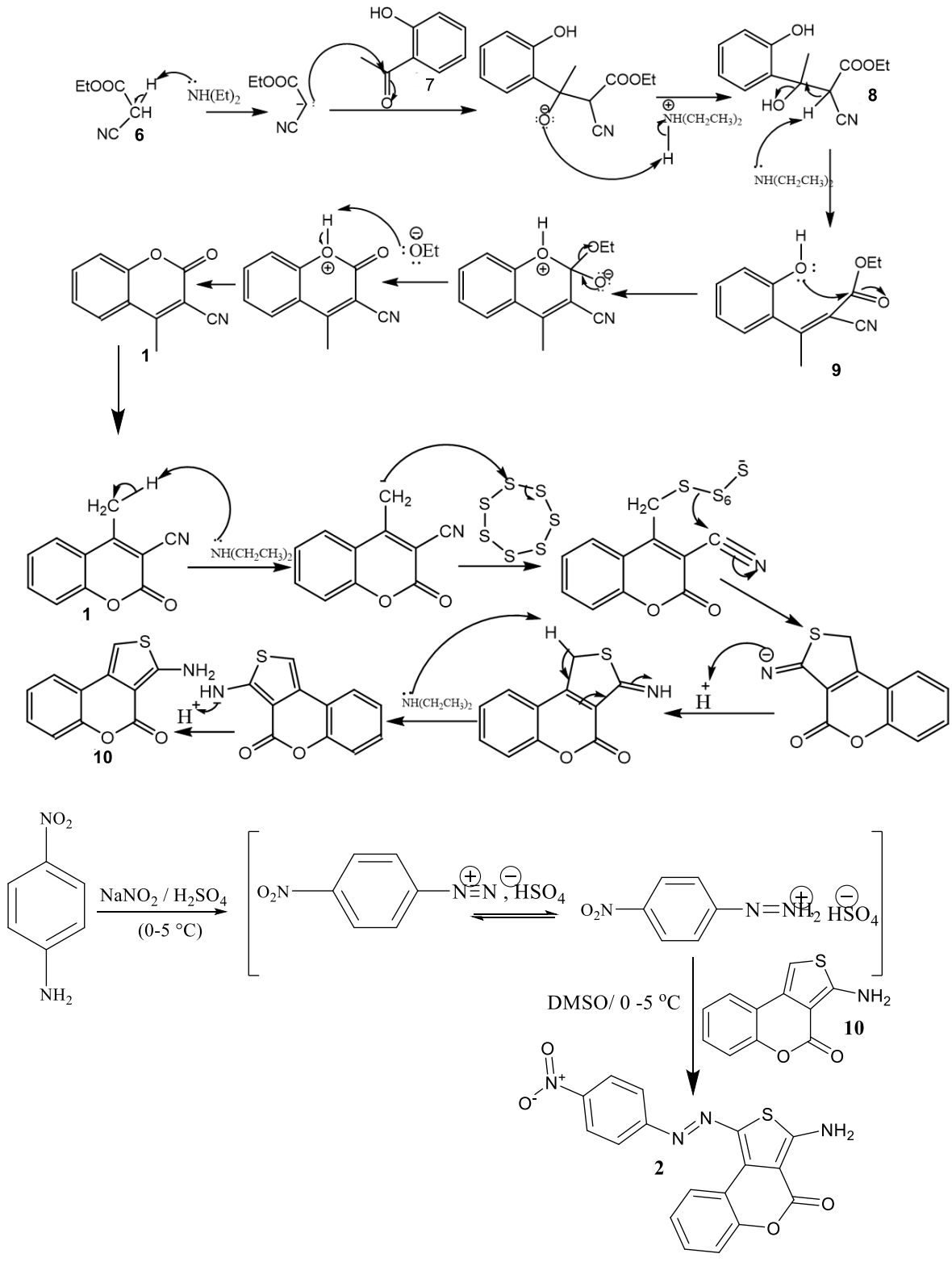


Figure 1: reaction scheme for the preparation of compound **2**

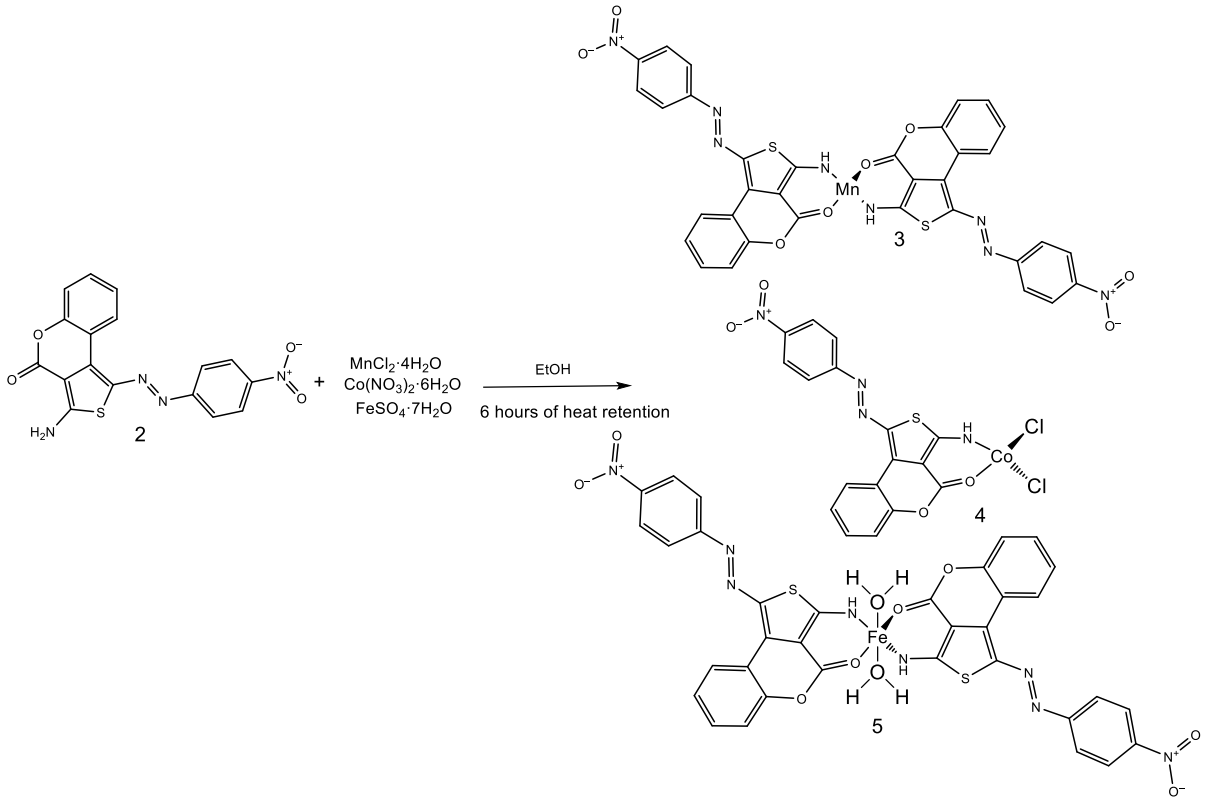


Figure 2: reaction scheme for the preparation of coordination compounds **3, 4** and **5**

The HRESI(+) mass spectrum of compound **2** (Supplementary Material, S1) showed the protonated molecular ion $[M+H]^+$ at m/z 367.05, in agreement with the proposed formula (calcd 366.04 g/mol; $C_{17}H_{10}N_4O_4S$). The UV-Visible spectrum (ethanol) displayed two absorption bands at λmax = 266 nm (π→π* transitions of the aromatic rings) and 318 nm (n→π* transitions of the azo/carbonyl chromophoric system), consistent with values reported for structurally related heterocyclic azo dyes [12].

The FT-IR spectrum (**Fig. 3**) confirmed the proposed structure: symmetric and asymmetric N-H stretching of the free primary amine at 3344 and 3311 cm^{-1}, lactone carbonyl (C=O) stretching at 1686 cm^{-1}, aromatic C=C stretching at 1585 cm^{-1}, the azo bridge (N=N) at 1416 cm^{-1}, and asymmetric nitro-group (NO_2) stretching at 1341 cm^{-1} [13,14]. A complex absorption envelope between 3480 and 3400 cm^{-1}, most likely arising from overlapping conjugated O-H (enol tautomer) and imine (=NH) signals, points to partial azo-hydrazone tautomerism in the solid state.

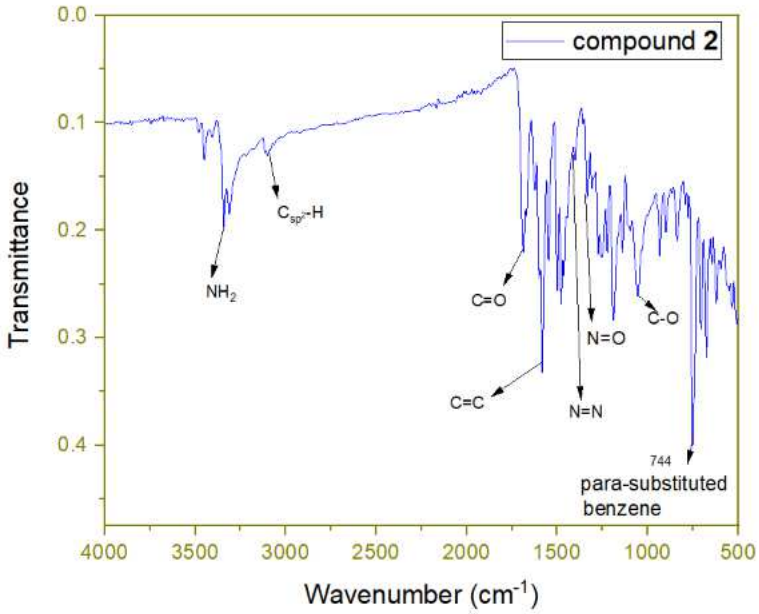


Figure 3 : FT-IR spectrum of compound **2** with band assignments

The ^{1}H NMR spectrum (DMSO-d6) (**Fig. 4**) confirmed successful diazo coupling through the disappearance of the amine signal of 4-nitroaniline (6.71 ppm) and of the H-9 singlet of the 2-aminothiophene precursor (6.87 ppm), replaced by a new set of signals: the residual thiophene amine (2-NH_2) as a singlet at 7.75 ppm, the coumarin-ring protons at 7.83 (H-8, dd), 7.32 (H-6, m) and 7.17-7.19 ppm (H-5/H-7, m), and the nitrophenyl-ring protons at 7.85 (H-14/H-14′) and 6.86 ppm (H-13/H-13′). The ^{13}C NMR spectrum (15 signals) showed shielding of C-2′ (118.1→98.3 ppm), C-8′ and C-9, attributable to the neighbouring amine, and marked deshielding of the nitrophenyl carbons C-13/13′, C-14/14′ and C-15 (135.8→151.3 ppm), consistent with the electron-withdrawing nitro substituent. Two-dimensional experiments (HSQC, HMBC, COSY ^{1}H-^{1}H cf. Supplementary Material) allowed too strong reconstruction of the molecular skeleton, notably through the HMBC correlation between 2-NH_2 (7.75 ppm) and C-2′ (98.3 ppm), which confirms connectivity across the azo bridge. The powder X-ray diffractogram of compound **2** showed intense, well-resolved peaks, consistent with a crystalline compound.

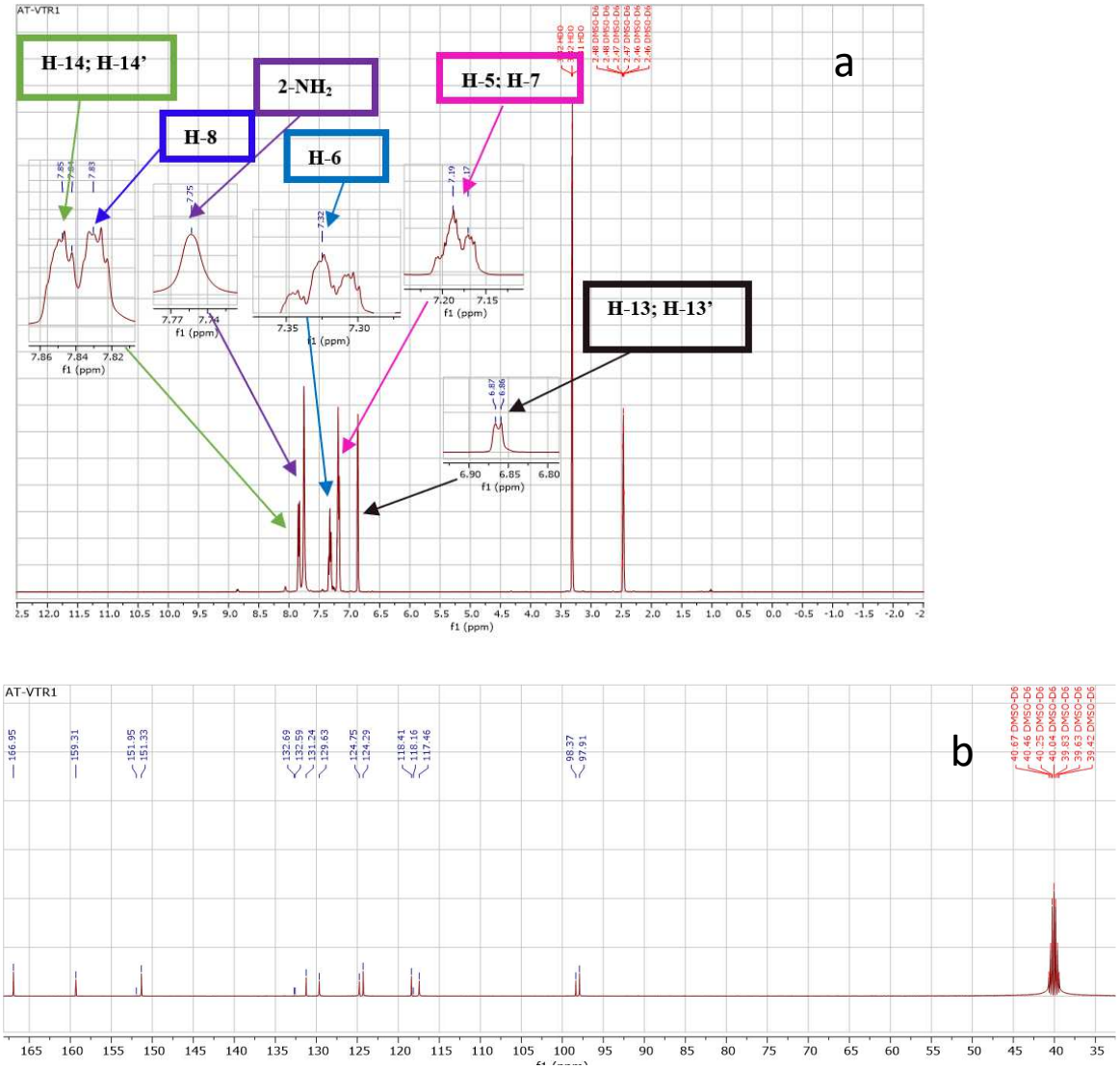


Figure 4: 1H (a) and 13C (b) NMR spectra of compound **2**, DMSO-*d6*, 400 MHz

Structural characterisation of the metal complexes

The UV-Vis spectra of the three complexes show a consistent bathochromic shift of both bands of free compound **2** ($\pi \rightarrow \pi^*$: 266→280-283 nm; $n \rightarrow \pi^*$: 318→364-368 nm), together with new ligand-to-metal charge-transfer bands (454-460 nm) and weak d-d transitions characteristic of each metal ion (567/679 nm for compound **3**, 534 nm for compound **4**), consistent with the extension of π-conjugation induced by coordination [15].

FT-IR spectroscopy (**Fig. 5**) provides direct evidence for coordination through the lactone oxygen and the deprotonated aromatic amine nitrogen in all three complexes. The two N-H_2 bands of the free

ligand (3344/3311 cm^{-1}) disappear and are replaced by a single N-H band (3265, 3326 and 3249 cm^{-1} for compound **3**, **4** and **5**, respectively), consistent with deprotonation of the primary aromatic amine upon complexation [16]. The lactone carbonyl shifts from 1686 cm^{-1} in the free ligand to 1718 cm^{-1} (**3**), 1675 cm^{-1} (**4**) and 1670 cm^{-1} (**5**), confirming the involvement of the carbonyl oxygen in coordination. The azo band, by contrast, remains unchanged at 1416 cm^{-1} in all three complexes, indicating that the azo bridge does not participate in metal binding. New low-frequency bands (528/400 cm-1 for compound **3**; 521 cm^{-1} for compounds **4** and **5**) are assigned to M-X stretching vibrations (M-N/O/Cl) [17,18]. For compound **5**, a broad band between 3422 and 3249 cm^{-1} associated with a bending mode at 842 cm^{-1} indicates the presence of coordinated water molecules.

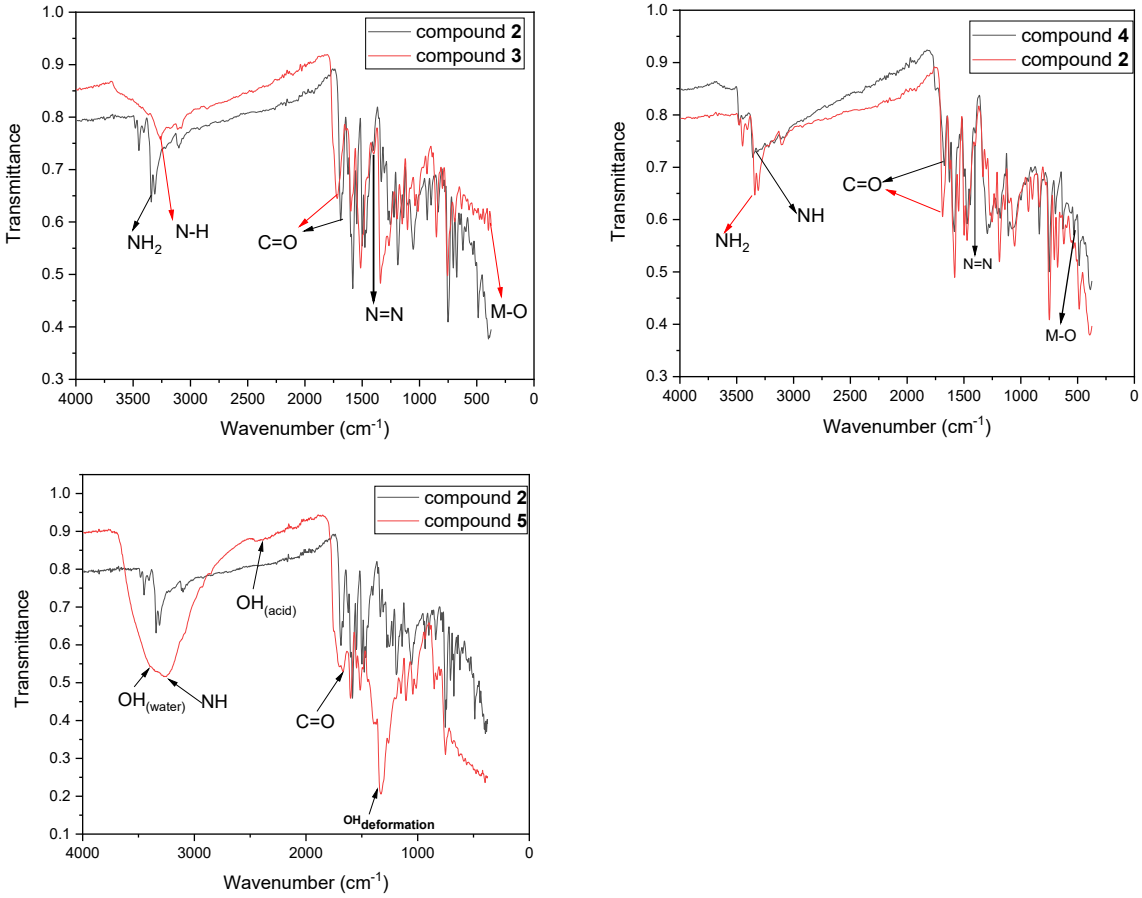
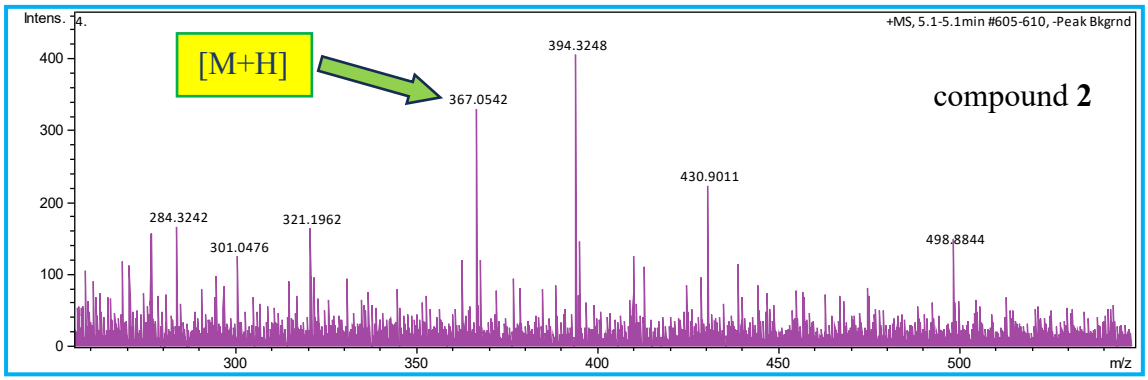
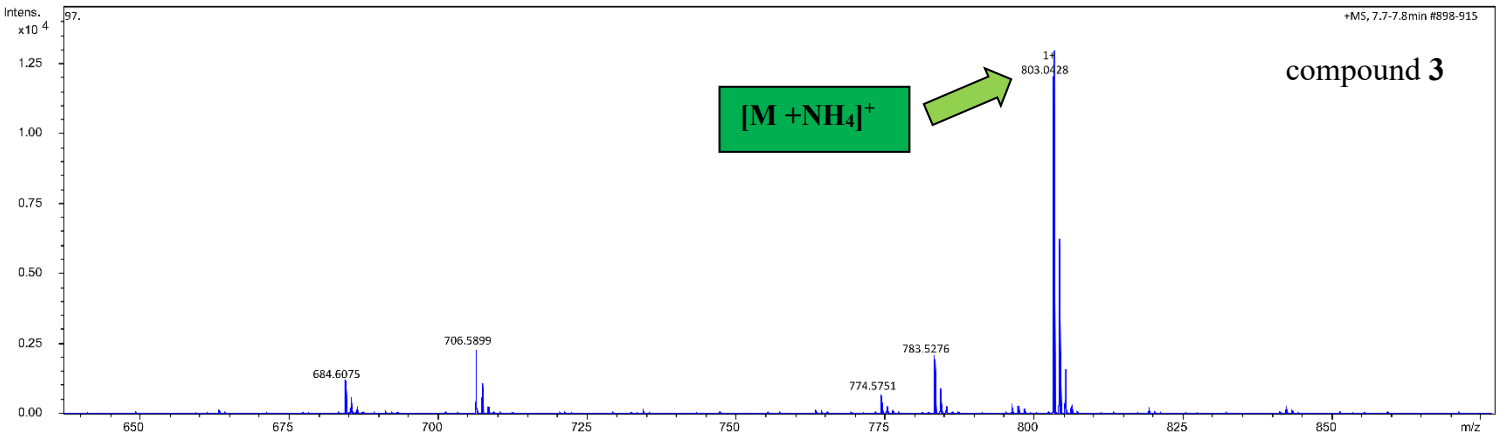


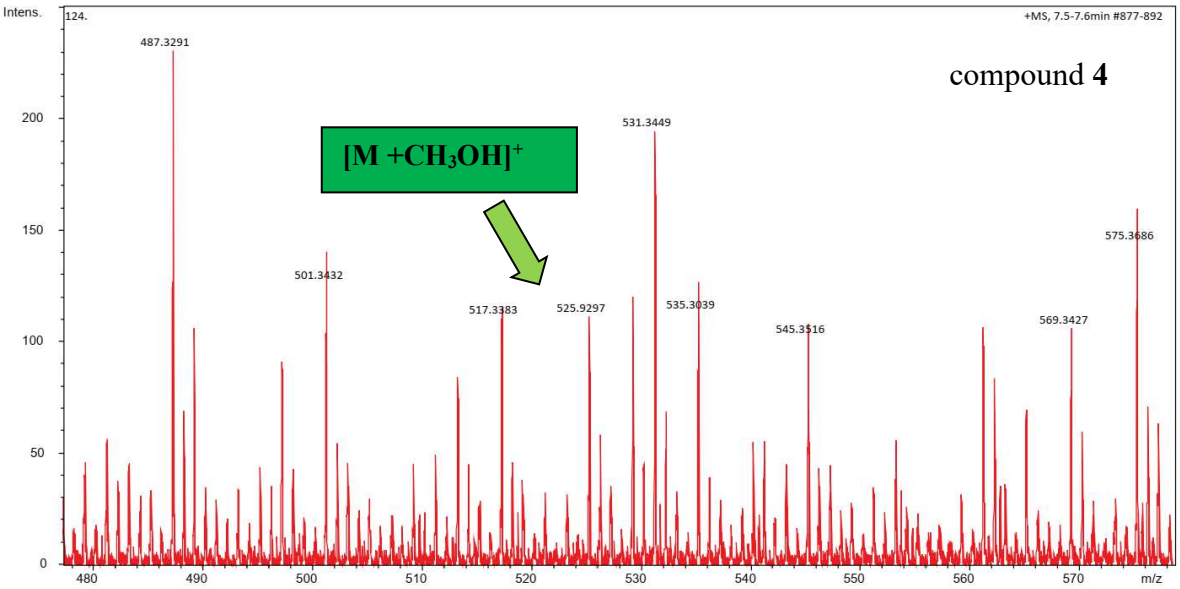
Figure 5 : Overlaid FT-IR spectra of compound **2** and the three complexes

HRESI mass spectrometry (**Fig. 6**) confirmed the proposed stoichiometries: a 2:1 (**2**:M) ratio for compound **3** ($[MnC_{34}H_{22}N_9O_8S_2]^+$, m/z 803.0428) and for compound **5** ($Fe(C_{34}H_{20}N_8O_9S_2)(H_2O)_2$, m/z

872.092), and a 1:1 ratio for compound **4** ($Co(C_{17}H_9N_4O_4S)(Cl)_2$, m/z 525.9297). For compound **4**, two additional fragment ions $[Co(Cl)_2+CH_3OH+H]^+$ (m/z 111.9245) and $[CoCl+NH_4]^+$ (m/z 161.9543) provide direct evidence for the involvement of chloride ions in the coordination sphere.







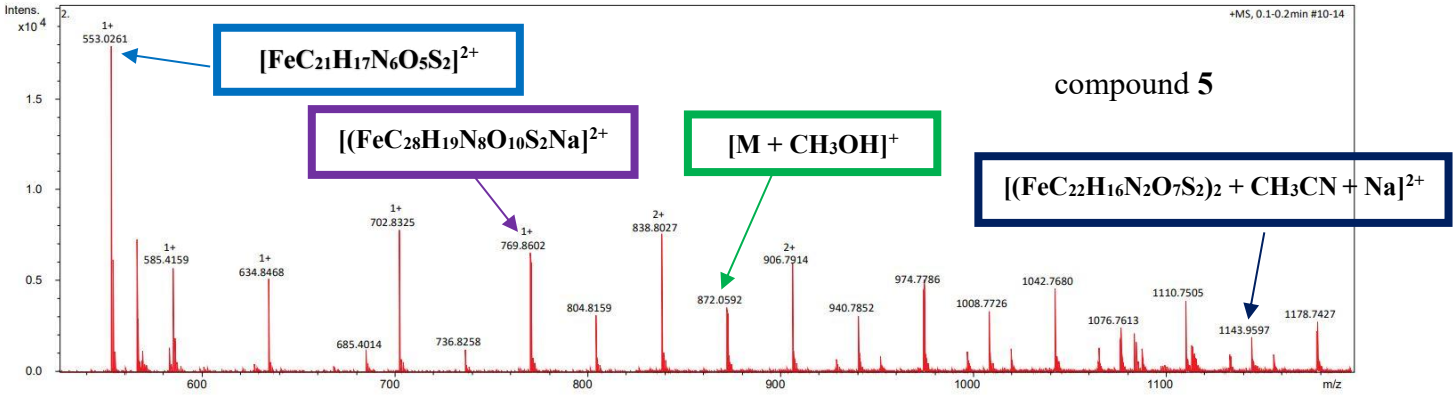


Figure 6: HRESI(+) mass spectra of compounds **2**, **3**, **4** and **5**

The ^{1}H and ^{13}C NMR signals in the diamagnetic region (Supplementary Material) retain the overall pattern of the free ligand, with minor diagnostic shifts: 2-NH_2 (7.75→7.74 ppm in the compound **3**; 7.75/7.76→7.75/7.77 ppm in the compound **4**) and splitting of the C-3 (166.9 ppm) and C-2 (159.3 ppm) signals in the compound **3**, consistent with coordination of the heteroatoms attached to these carbons. An unassigned HSQC correlation at 3.13 ppm in the compound **3** spectrum was attributed to coordinated water. The powder diffractograms of the three complexes are clearly distinct from that of free compound **2**, confirming the formation of new crystalline phases upon complexation.

The powder XRD pattern of VTR (2θ = 5 -130°, CuKα, Rigaku SmartLab, Bragg-Brentano geometry) shows sharp, well-resolved peaks, confirming the crystalline character of the ligand; this profile served as the reference against which the effect of complexation was assessed [32,33].

The diffractograms of compounds **3**, **4** and **5** are each clearly distinct from that of **2** : the free-ligand peaks disappear and are replaced by new reflections specific to each complex, with no residual peaks attributable to either the ligand or the starting metal salt. This change confirms the formation of new, pure crystalline phases and is consistent with the geometries proposed from the UV-Vis and IR data: tetrahedral for **3** and **4**, octahedral for **5** [32,34].

DFT study: frontier orbitals and global reactivity descriptors

DFT-optimised geometries (**Fig. 7**) indicate a tetrahedral coordination for compound **3** (two bidentate compound **2** units surrounding Mn^{2+}) and for compound **4** (one bidentate compound **2** unit and two

axial Cl^- ligands surrounding Co^{2+}), and an octahedral geometry for compound **5** (two bidentate compound **2** units and two axial water molecules surrounding Fe^{2+}), consistent with the d5, d7 and d6 electronic configurations, respectively, and with the spectroscopic data discussed above.

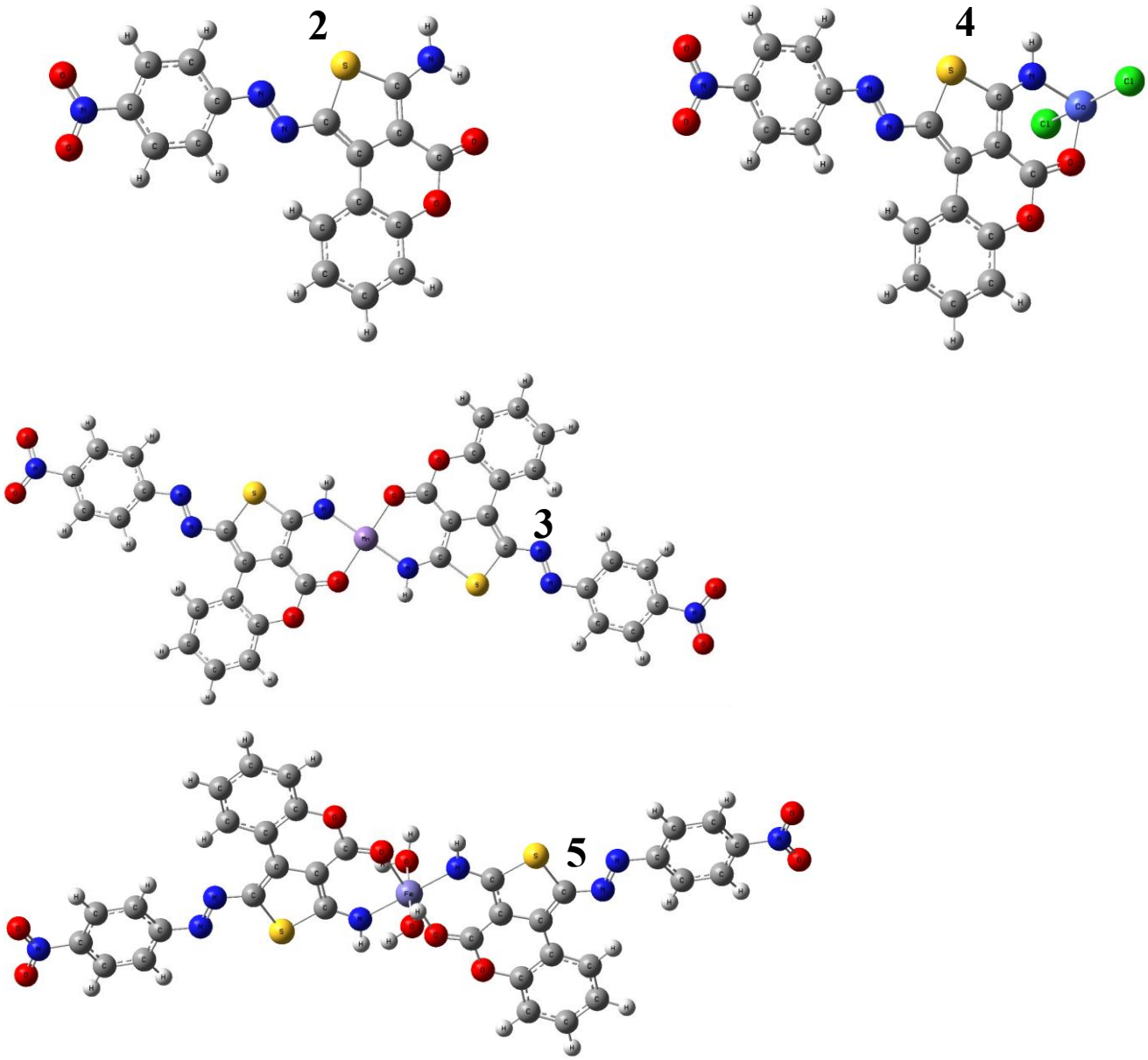
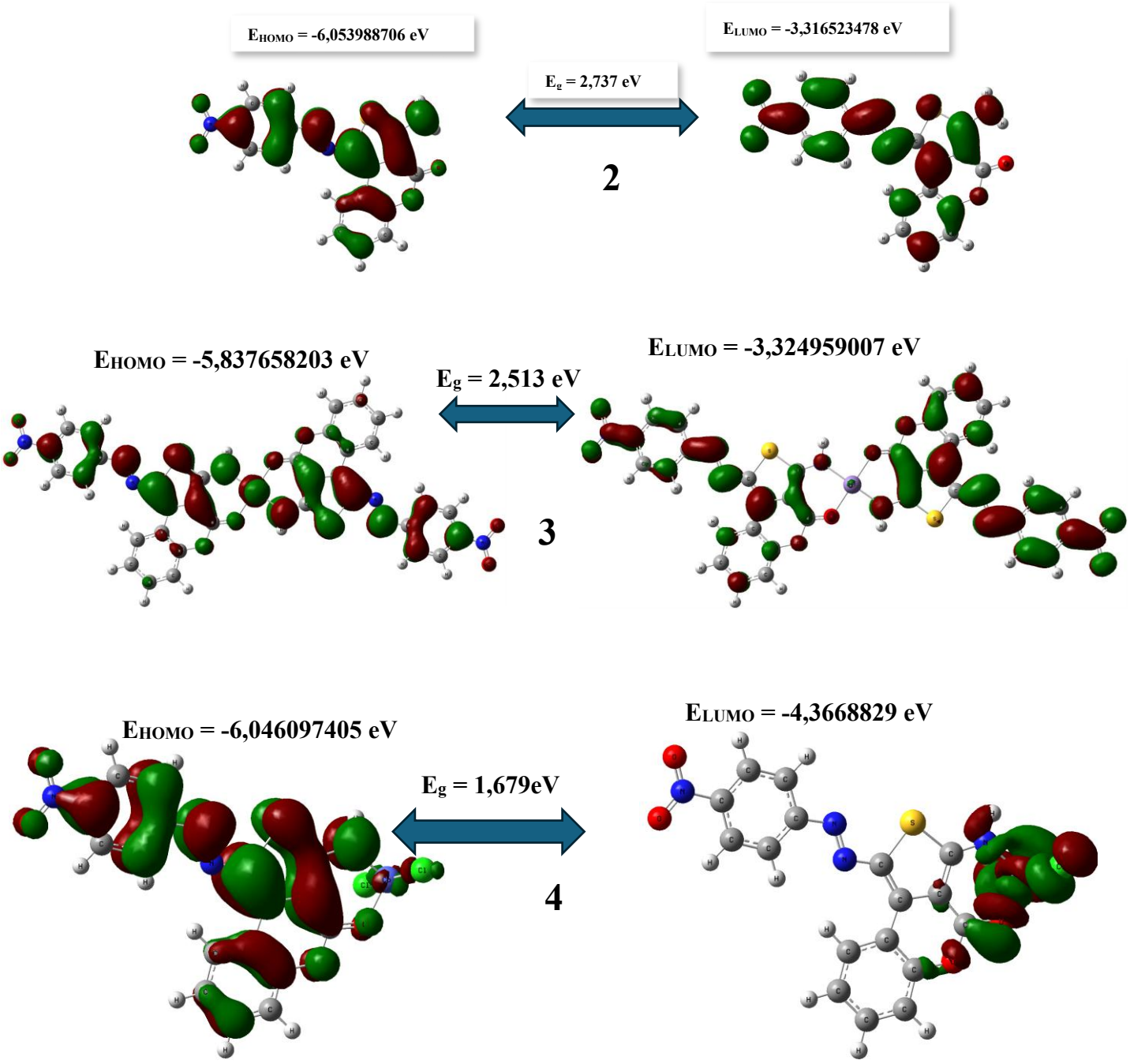


Figure 7 : DFT-optimised structures (B3LYP/6-311++G(d,p)) of compounds **2**, **3**, **4** and **5**

The HOMO of free compound **2** (EHOMO = -6.054 eV) is delocalised over the coumarin-thiophene-azo system, whereas the LUMO (ELUMO = -3.317 eV) is concentrated on the nitrophenyl ring and the adjacent azo bridge a signature of intramolecular push-pull charge transfers typical of para-nitro-

substituted azo dyes. An electronic architecture of this type has previously been described by Ayare et al. for a series of coumarin-cored, thiophene-bridged disperse azo dyes, whose photostability and antimicrobial activity on dyed fabric were rationalised using global reactivity descriptors derived from conceptual DFT, with a direct relationship reported between HOMO-LUMO (**Fig. 8**) gap narrowing and the intensity of the measured antimicrobial activity [22].



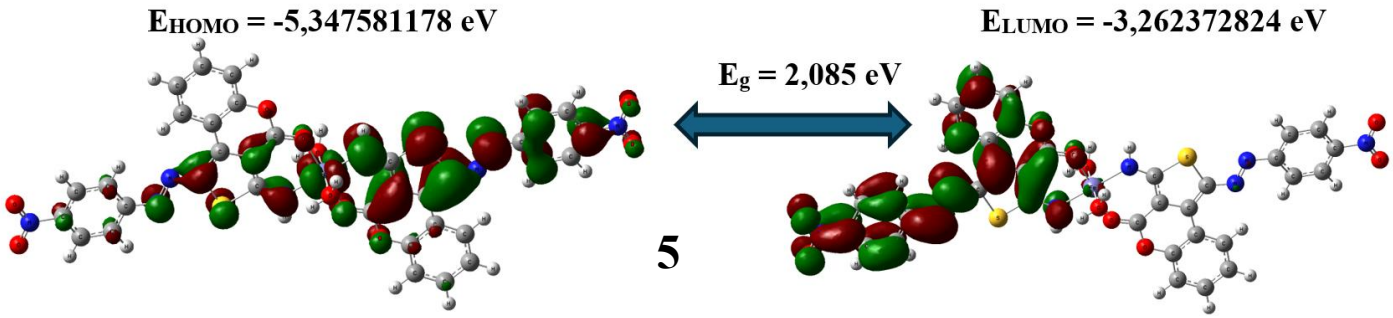


Figure 8 : Frontier molecular orbital diagrams (HOMO/LUMO) of compound **2**, **3**, **4** and **5**

Complexation systematically narrows the HOMO-LUMO gap (ΔE) relative to the free ligand (2.737 eV), in the order **4** (1.679 eV) < **5** (2.085 eV) < **3** (2.513 eV) < **2**. For compound **4**, the LUMO migrates almost entirely onto the Co-Cl_2 coordination sphere, a shift we attribute to the weak-field character of the chloride ligands, which lowers the metal d-levels in the tetrahedral environment. For compound **5**, the LUMO shows a notable asymmetric distribution, localised on only one of the two equivalent compound **2**- fragments; we attribute this to a Jahn-Teller-type distortion or to an uneven vibronic coupling between the two ligand units and the axial water molecules [19]. For the compound **3**, by contrast, the HOMO and LUMO remain symmetrically delocalised over both ligand fragments, consistent with the weak-field, high-spin, d5 character of Mn(II) in a tetrahedral N,O environment.

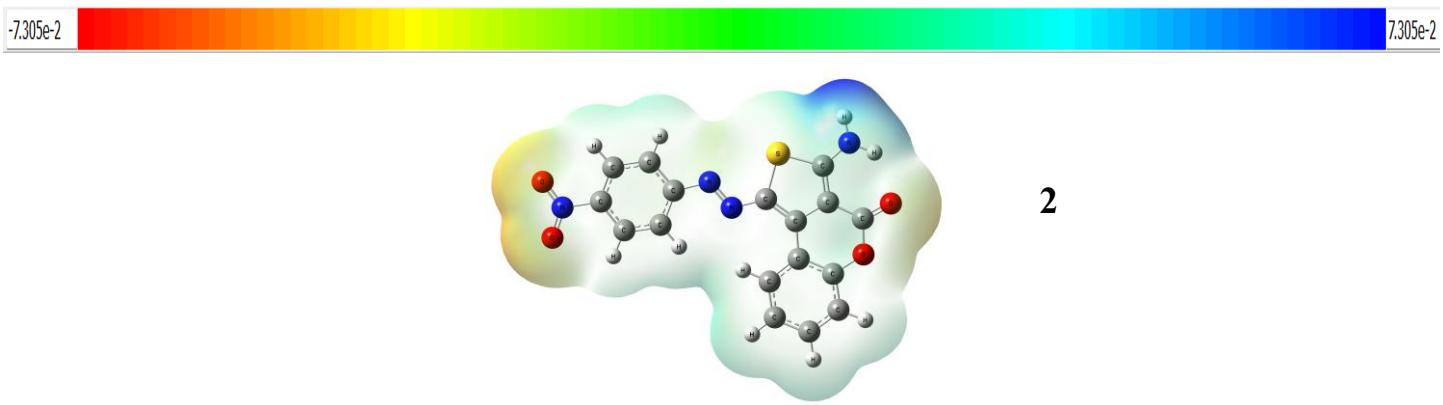
The global reactivity descriptors (**Table 1**), calculated within the conceptual DFT formalism [20,21], confirm this hierarchy: chemical hardness decreases in the order **2** (1.369 eV) > **3** (1.256 eV) > **5** (1.043 eV) > **4** (0.840 eV), while the electrophilicity index of compound **4** (ω = 16.143 eV) is roughly twice that of the other three compounds (8.0-8.9 eV), a direct reflection of LUMO localisation at the Co-Cl_2 site.

Table 1. Global reactivity descriptors of compound **2** and its Mn(II), Co(II) and Fe(II) complexes

Compound	I (eV)	A (eV)	χ (eV)	μ (eV)	η (eV)	S (eV^{-1})	ω (eV)
2	6.054	3.317	4.685	-4.685	1.369	0.365	8.019
3	5.838	3.325	4.581	-4.581	1.256	0.398	8.353
4	6.046	4.367	5.206	-5.206	0.840	0.596	16.143
5	5.348	3.262	4.305	-4.305	1.043	0.480	8.888

This high electrophilicity of the compound **4**, however, does not translate into superior antibacterial activity (see below), a point worth emphasising: unlike the series reported by Ayare et al., in which HOMO-LUMO gap narrowing directly tracked a measured gain in activity on dyed fabric [22], the present system comprises three coordination spheres of different nature (tetrahedral N,O,Cl_2; bis-chelated tetrahedral N,O; octahedral N,O,H_2O). It should be noted that these electronic descriptors capture the intrinsic propensity of the isolated molecule to accept electrons but does not, on its own, predict membrane permeability or complementarity with a biological target a limitation increasingly discussed in the recent literature on metal-azo complexes [23,24]. The pronounced electrophilic character and narrow gap of compound **4** nonetheless bring this compound closer to a push-pull chromophore with strong acceptor character, which could justify, in a follow-up study, an evaluation of its optoelectronic properties (nonlinear absorption, dye-sensitised solar cell response) in the manner already applied to other donor-acceptor azo-coumarin dyes [22].

Molecular electrostatic potential (MEP) (**Fig. 9**) maps locate the most electron-rich regions of compound **2** on the lactone oxygen and, to a lesser extent, on the azo nitrogen atoms, consistent with the N, O coordination mode deduced from the IR and NMR data. In all three complexes, a new region of positive potential appears centred on the metal diffuse and shared between the two chloride ligands in compound **4**, sharply localised around the iron centre and its two axial water molecules in compound **5** while the nitro group retains an unchanged signature in every case, confirming its non-participation in coordination.



2

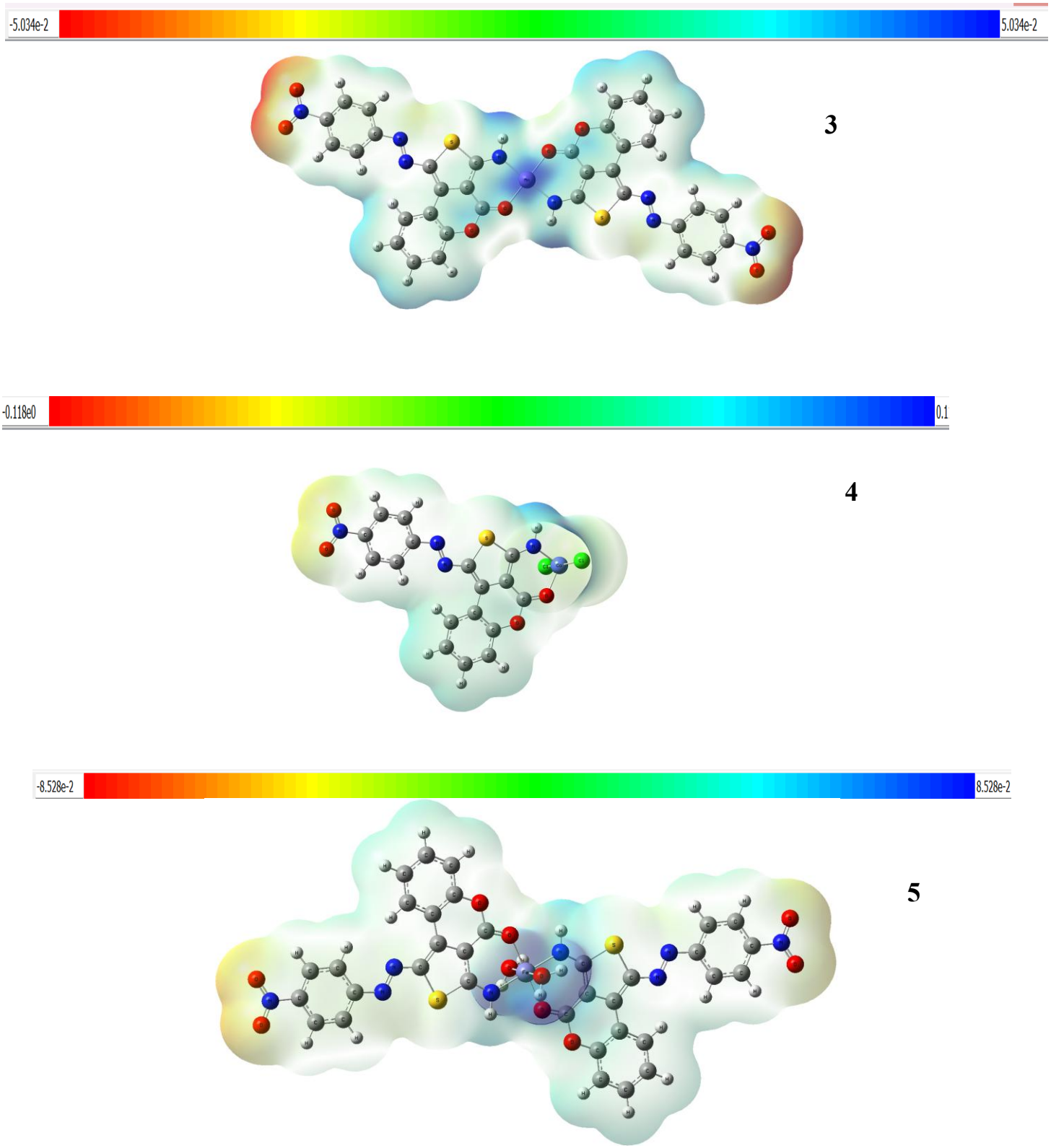


Figure 9: molecular electrostatic potential (MEP) maps of compounds **2**, **3**, **4** and **5**

Molecular docking against bacterial enzymatic targets

The molecular docking analysis suggests that metal coordination substantially influences the interaction of the compounds with selected bacterial targets, although the results should be interpreted cautiously. The docking scores obtained for compounds 2-5 and ciprofloxacin against the three selected bacterial targets are summarised in **Table 2.** Against 7AB4 (*E. coli*) and 1MWT (*S. aureus*), the Mn(II) complex 3 displayed the most favorable docking scores (−8.70 and −7.02 kcal/mol, respectively), indicating potentially enhanced binding compared with the parent ligand. However, its interaction with 7AB4 is less conclusive because it did not engage the catalytic residues and exhibited an RMSD of 3.72 Å, above the commonly adopted 2 Å reliability threshold. In contrast, its interactions with Ser403 and Ser462 in 1MWT provide a more structurally consistent binding mode. For 4NG2 (*P. aeruginosa*), the generally weak or unfavorable scores and the absence of interactions with the key binding-site residues suggest limited suitability of this compound series for LecB inhibition. Overall, the docking results support a possible beneficial effect of Mn(II) coordination on target recognition, particularly against bacterial DNA gyrases, but they should be regarded as supportive evidence rather than definitive proof of the underlying antibacterial mechanism.

Table 2. Docking scores (kcal/mol) of compounds 2, 3, 4, 5, and ciprofloxacin against three bacterial targets

Compound	7AB4 (*E. coli*)	1MWT (*S. aureus*)	4NG2 (*P. aeruginosa*)
2	-7.35	-5.42	-4.73
3	-8.70	-7.02	+9.72
4	-7.90	-5.30	-2.66
5	-5.61	-5.54	+0.26
Ciprofloxacin	-7.29	-5.43	+3.57

Antibacterial activity and in silico/in vitro correlation

MIC values (**Table 3**) ranged from 16 to 128 µg/mL, these values are typical for related azo-thienochromenone metal complexes against the same bacterial species [9,25]. Compound **3** emerged as the most active compound of the series: MIC = 16 µg/mL against *E. coli and S. aureus*, matching ciprofloxacin on *E. coli*, and the only complex with a determined MBC against *E. coli* (128 µg/mL). Compound **4** was active against *S. aureus* (MIC = 16 µg/mL) but markedly less effective against *E.*

coli (MIC = 128 µg/mL), consistent with the additional permeability barrier imposed by the outer membrane of Gram-negative bacteria. Compound **5** was the only compound with a determined MBC against two strains *P. aeruginosa* and *S. aureus* (both at 64 µg/mL) and the only complex strictly bactericidal against *P. aeruginosa* (MBC/MIC = 1), a profile we attribute to the Fe^{2+}/Fe^{3+} redox cycle generating reactive oxygen species at the bacterial membrane [26]. The free ligand **2** remained moderately active across all strains (MIC = 32-64 µg/mL) without a determined MBC, confirming that metal coordination improved activity two- to four-fold in every case, consistent with Tweedy's chelation theory [8] and with recent reports on related azo-metal systems [9,10,27].

Table 3. Minimum inhibitory (MIC) and bactericidal (MBC) concentrations (µg/mL)

Compound	MIC Pa	MBC Pa	MIC Sa	MBC Sa	MIC Ec	MBC Ec
2	64	-	32	-	64	-
3	32	-	16	-	16	128
4	32	-	16	-	128	-
5	64	64	16	64	128	128
Ciprofloxacin	8	16	8	16	16	32

Comparison of docking scores with experimental MIC values (**Table 4**) revealed a partial but informative qualitative agreement. Compound **3** showed the strongest concordance: the best docking score on both gyrase targets and the best experimental MIC on the corresponding strains, with near-equivalence to ciprofloxacin against *E. coli* at both levels (docking: -8.70 vs -7.29 kcal/mol; MIC: 16 vs 16 µg/mL). Such a degree of in silico/in vitro agreement across an entire compound series is uncommon and has recently been documented for structurally related heterocyclic metal complexes [28-30].

Two notable discrepancies were observed. compound **4** obtained the second-best score on 7AB4 (-7.90 kcal/mol) but showed weak activity against *E. coli* (MIC = 128 µg/mL), which we attribute to the absence of catalytic-residue contacts in its docking pose, combined with reduced membrane penetration in Gram-negative bacteria. Compound **5**, with the weakest 7AB4 score (-5.61 kcal/mol),

accordingly showed no notable inhibition of *E. coli* (MIC = 128 µg/mL); its bactericidal activity against *P. aeruginosa* and *S. aureus*, however, was not predicted by the repulsive score obtained on 4NG2, suggesting a secondary, redox-mediated mechanism independent of the enzymatic targets examined here [26]. On 4NG2, the correlation was negatively consistent: all compounds obtained unfavourable scores, and the corresponding MIC values against *P. aeruginosa* were indeed the weakest of the series (32-64 µg/mL), correctly identifying this strain as the most refractory target for the compound **2** family.

Table 4. Comparison of docking scores and experimental MIC values on matching target/strain pairs

Compound	7AB4 score	MIC *E. coli*	1MWT score	MIC *S. aureus*	4NG2 score	MIC *P. aeruginosa*
2	-7.35	64	-5.42	32	-4.73	64
3	-8.70	16	-7.02	16	+9.72	32
4	-7.90	128	-5.30	16	-2.66	32
5	-5.61	128	-5.54	16	+0.26	64
Ciprofloxacin	-7.29	16	-5.43	8	+3.57	8

Taken together, these results indicate that compound 3 combines the most favourable electronic profile (moderate HOMO-LUMO gap, symmetric delocalisation of the frontier orbitals), the strongest predicted affinity for both bacterial gyrase targets, and the best experimentally measured antibacterial activity of the series making it the most promising candidate to emerge from this study. Several methodological caveats nonetheless deserve mention: the relatively high RMSD values obtained for compound **3** across the three targets (3.15-4.86 Å) call for validation by molecular dynamics simulation before mechanistic conclusions can be drawn, and the absence of direct engagement with catalytic residues on 7AB4 tempers the interpretation of its favourable docking score. All complexes remained less active than ciprofloxacin (MIC 8-16 µg/mL), an expected outcome for first-generation metal complexes not yet optimised.

Conclusions

A nitrophenyl-substituted azo-thienochromenone ligand, compound **2**, was obtained by diazo coupling of 4-nitroaniline onto an aminothienochromenone precursor prepared according to a modified Gewald route, and used to prepare three new Mn(II), Co(II) and Fe(II) complexes. The nitrophenyl-coupled ligand corresponds structurally to a disperse azo dye previously reported in the literature; the present study reports, for the first time, its behaviour as a coordinating ligand. The spectroscopic data converge on bidentate N,O coordination through the lactone carbonyl oxygen and the deprotonated aromatic amine, with the azo bridge and the nitro group remaining uncoordinated. DFT calculations reveal a systematic narrowing of the HOMO-LUMO gap upon complexation, most pronounced for compound **4** owing to LUMO migration toward the Co-Cl_2 sphere, and an asymmetric LUMO distribution in **5** attributed to vibronic or Jahn-Teller-type effects.

Molecular docking against the E. coli and *S. aureus* DNA gyrases identifies compound **3** as the best binder of the series, a prediction corroborated by in vitro susceptibility testing, in which compound **3** displayed the lowest overall MIC values (16 µg/mL against both organisms). Compound **5** displayed a distinct bactericidal profile, associated with a redox mechanism, against *P. aeruginosa*. These findings support the interest of the azo-thienochromenone scaffold as a viable platform for metal-based antibacterial agents, and underline the value of an approach combining DFT-derived reactivity descriptors, structured docking and experimental microbiology for candidate prioritisation an approach already fruitful for other families of heterocyclic azo dyes [22]. Future work should address molecular-dynamics validation of the most promising docking poses, broader susceptibility screening against multidrug-resistant clinical isolates, cytotoxicity profiling to establish a selectivity index for the most active complexes, and, given the pronounced push-pull character of the compound **2** chromophore, complementary optoelectronic characterisation (nonlinear absorption, dye-sensitised solar-cell response) that could position this scaffold as a multifunctional material beyond its antibacterial application.

Materials and methods

Materials and instrumentation

All reagents and solvents were of analytical grade (Sigma-Aldrich, Merck, Fisher Scientific) and were used without further purification unless otherwise stated. Reaction progress was monitored by thin-layer chromatography (silica gel 60F254, Merck), using hexane/ethyl acetate (50:50, v/v) as eluent, with visualisation by spraying with 10% HCl and heating at 90-100 °C.

HRESI mass spectra were recorded in positive-ion mode on a Bruker MicrOTOF-Q spectrometer coupled to a Dionex Ultimate 3000 LC system (École Normale Supérieure de Yaoundé), and processed with Bruker DataAnalysis 4.3. UV-Visible spectra (200-800 nm, 1 cm quartz cuvette, ethanol) were recorded on a Thermo Scientific Genesys 10S spectrophotometer (URCNGE, University of Dschang). FT-IR spectra were recorded in ATR mode (germanium crystal, 4000-400 cm^{-1}, extended to 300 cm^{-1} for far-IR metal-ligand vibrations) on a Thermo Scientific Nicolet iS5 instrument (University of Yaoundé I). ^{1}H and ^{13}C NMR spectra (400 and 100 MHz, respectively, DMSO-d6), including 2D experiments (HSQC, HMBC, COSY ^{1}H-^{1}H), were recorded on a JEOL ECZ 400 spectrometer (Carleton University, Ottawa, Canada). Powder diffractograms were collected on a Rigaku SmartLab diffractometer (Cu Kα radiation, 40 kV/135 mA, 2θ = 5-130°) at the University of Finland.

Synthetic procedures

Synthesis of 4-methyl-2-oxo-2H-chromene-3-carbonitrile

1-(2-Hydroxyphenyl)ethan-1-one (2′-hydroxyacetophenone, 13.6 g, 0.10 mol) was dissolved in absolute ethanol (30 mL) and treated with ethyl 2-cyanoacetate (11.3 g, 0.10 mol). The mixture was cooled to 0-5 °C and diethylamine (7.3 g) was added dropwise over 10 min while keeping the temperature below 5 °C. After stirring for 2 h at 0-5 °C, the mixture was allowed to warm to room temperature, and the resulting pale-green crystals were collected by filtration, washed with cold ethanol and dried (12.2 g, 65.9%).

Synthesis of 3-amino-4*H*-thieno[3,4-c]chromen-4-one

This compound was prepared following an adaptation of the modified Gewald route previously described by our group for access to 3-amino-4*H*-thieno[3,4-c]chromen-4-one derivatives [6,7].The 3-amino-4*H*-thieno[3,4-c]chromen-4-one (4.65 g, 25.1 mmol) was dissolved in absolute ethanol (30 mL) and treated with elemental sulfur (1.22 g, 38.2 mmol). The mixture, heated to 60 °C, received a solution of diethylamine (6 mL) in ethanol (5 mL) added dropwise over 10 min, and was then maintained at 45-50 °C for 6 h with TLC monitoring. The resulting yellow precipitate was filtered, washed with cold ethanol and recrystallised from ethanol (4.65 g, ca. 93%), a yield consistent with the values reported in this earlier work.

Synthesis of the azo ligand

4-Nitroaniline (0.64 g, 4.63 mmol) was dissolved in DMSO (5 mL) and cooled to 0-5 °C. Concentrated sulfuric acid (5 mL) was added dropwise over 30 min at 0-5 °C, followed by portion-wise addition of sodium nitrite (1.2 g) until a positive starch-iodide test confirmed complete diazotisation. A solution of 3-amino-4H-thieno[3,4-c]chromen-4-one (1.0 g, 4.61 mmol) in DMSO (5 mL) was then added dropwise at 0-5 °C, and the mixture was stirred for 30 min. The reaction was neutralised with 10% aqueous sodium acetate to pH ≈ 5-6, diluted with cold water (50 mL), and left to stand for 30 min. The resulting brown precipitate was filtered, washed with cold water and air-dried, affording compound **2** (1.96 g crude; a further 0.08 g was recovered from the filtrate after recrystallisation from ethanol). Rf = 0.6 (hexane/ethyl acetate, 50:50); soluble in DMSO, partially soluble in ethanol. As noted above, this compound corresponds structurally to the previously reported disperse dye of Al-Mousawi and El-Apasery [11]; the spectroscopic data recorded here (HRESI-MS, UV-Vis, FT-IR, 1D/2D NMR, powder XRD) are nonetheless reported in the Supplementary Material, as they underpin the coordination chemistry and computational analysis that follow.

General procedure for the synthesis of the metal complexes

Compound **2** (0.18 g, 0.50 mmol) was dissolved in methanol (10 mL). The corresponding metal salt manganese(II) chloride tetrahydrate (0.10 g, 0.50 mmol) for compound **3**, cobalt(II) chloride hexahydrate (0.15 g, 0.50 mmol) for compound **4**, or iron(II) sulfate heptahydrate (0.14 g, 0.50 mmol)

for compound **5** was dissolved separately in methanol (5 mL) and added dropwise to the ligand solution under stirring. Each mixture was refluxed at 70 °C for 6 h, filtered hot, and the filtrate was allowed to evaporate slowly at room temperature over 14 days. The resulting maroon precipitates were collected by filtration (compound **3**: 45 mg; compound **4**: 55 mg; compound **5**: 58 mg).

Compound **3**: HRESI(+) m/z = 803.0428 $[M+NH_4]^+$ (calcd 803.0413) for $[MnC_{34}H_{22}N_9O_8S_2]^+$. Compound **4**: HRESI(+) m/z = 525.9297 $[M+CH_3OH]^+$ (calcd 525.9316) for $Co(C_{17}H_9N_4O_4S)(Cl)_2$, M = 493.91 g/mol. Compound **5**: HRESI(+) m/z = 872.0592 $[M+CH_3OH]^+$ (calcd 872.0617) for $Fe(C_{34}H_20N_8O_9S_2)(H_2O)_2$, M = 840.04 g/mol.

Computational methods

DFT calculations

Geometry optimisations were carried out at the DFT level using the B3LYP hybrid exchange-correlation functional with the 6-311++G(d,p) basis set for all atoms, using Gaussian 09 (Revision D.01-SMP) [40] with structures built in GaussView 6.0. The absence of imaginary frequencies confirmed that all optimised geometries corresponded to genuine energy minima. The frontier molecular orbitals (HOMO, LUMO), the HOMO-LUMO gap (ΔE), the global reactivity descriptors (ionisation potential I, electron affinity A, electronegativity χ, chemical potential μ, hardness η, softness S, electrophilicity index ω) [20,21] and the molecular electrostatic potential (MEP) maps (isodensity surface ρ = 0.0004 a.u.) were derived from the optimised geometries.

Molecular docking

Docking studies were performed with Molecular Operating Environment (MOE 2019.0102) in semi-flexible mode (rigid protein, flexible ligand), with results visualised in Discovery Studio 2019. Three bacterial protein targets were retrieved from the Protein Data Bank (https://www.rcsb.org/): the GyrB subunit of *E. coli* DNA gyrase (PDB: 7AB4), *S. aureus* DNA gyrase (PDB: 1MWT), and *P. aeruginosa* lectin LecB (PDB: 4NG2). Co-crystallised ligands and water molecules were removed prior to docking; partial charges were assigned and the energy of each receptor was minimised in

MOE before active-site selection. DFT-optimised geometries of compounds **2**, **3**, **4** and **5** (saved in sdf format) were used as docking ligands; ciprofloxacin, retrieved from PubChem, served as the reference inhibitor. Poses with an RMSD < 2 Å relative to the lowest-energy conformation were retained as geometrically reliable.

Antibacterial evaluation

Three reference bacterial strains were used: *Staphylococcus aureus* ATCC 25923 (Gram-positive), *Escherichia coli* ATCC 25922 (Gram-negative) and *Pseudomonas aeruginosa* 4C76110 (Gram-negative), selected to correspond to the organisms carrying the docking targets described above. Minimum inhibitory concentrations (MICs) were determined by broth microdilution in Mueller-Hinton broth (MHB) following the protocol of Tamokou et al. [25], adapted to CLSI standards, over a concentration range of 0.125 to 256 µg/mL; ciprofloxacin served as the positive control. Minimum bactericidal concentrations (MBCs) were determined by subculturing the contents of wells showing no visible growth onto Mueller-Hinton agar (MHA); the MBC was defined as the lowest concentration yielding no colony growth, or a single colony. All assays were performed in triplicate.

Declarations

Consent to Participate declaration : not applicable.

Consent to Publish declaration : not applicable.

Ethics declaration : not applicable.

Funding

This work was supported by the German Academic Exchange Service (DAAD; grant no. 91691265), the University of Dschang Research Grant Committee, and the Ministry of Higher Education of Cameroon. Additional support was provided by the DAAD through the Yaoundé-Bielefeld Graduate School of Natural Products with Antiparasite and Antibacterial Activities (YaBiNaPA; project no. 57316173).

Availability of data and materials

The datasets generated and/or analysed during the current study are available from the corresponding author on reasonable request.

Competing interests

The authors declare no competing interests.

Author contributions

Emmanuel Sopbué Fondjo, as supervisor and corresponding author, conceived and supervised the research project, coordinated the scientific activities, contributed to the interpretation and validation of the results, critically reviewed and revised the manuscript, and secured funding.

Victor Bertold Atedjong Tedjong conceived and coordinated the study, designed the synthesis and characterisation strategy for the ligand and its Mn(II), Co(II) and Fe(II) complexes, supervised and contributed to the DFT calculations and molecular docking analyses, participated in the interpretation and validation of the spectroscopic, computational and antibacterial results, and drafted and critically revised the manuscript.

Jean-de-Dieu Tamokou supervised the in vitro antibacterial investigations and contributed to the experimental design, interpretation and validation of the antibacterial results.

Steve Perin Dadem Kemgou contributed to interpretation of the experimental results, theoretical calculations, in vitro antibacterial assays, in silico molecular-docking studies, and preparation of the initial manuscript draft.

Sorelle Songmi Feuze contributed to the characterisation and interpretation of the spectroscopic data of the synthesised compounds and assisted in the critical review of the manuscript.

André Désiré Siéwé contributed to the characterisation of the synthesised compounds, particularly the analysis and interpretation of spectroscopic data, and participated in the critical review of the manuscript.

Apollinaire Tsopmo contributed to the scientific interpretation of the results, particularly with regard to the chemical and biological aspects of the study, participated in the acquisition and interpretation of the NMR spectroscopic data, and took part in the critical review and revision of the manuscript.

Peter Friedrich Wilhelm Simon contributed to the interpretation and discussion of the physicochemical and spectroscopic results and provided scientific input related to the characterisation of the synthesised compounds. He also contributed to the critical review of the manuscript.

Bruno Lenta Ndjakoue performed and/or contributed to the spectroscopic analyses of the synthesised compounds and to the interpretation of the corresponding experimental data.

Jules Roger Kuiate contributed to the scientific supervision and interpretation of the microbiological and antibacterial aspects of the study and participated in the critical review and revision of the manuscript.

All authors contributed to the scientific discussion of the results, read and approved the final version of the manuscript, and agreed to be accountable for the work.

Acknowledgements
Emmanuel Sopbué Fondjo warmly acknowledges DAAD funding (grant N° 91691265). The University of Dschang's research grant committee and the Cameroonian Ministry of Higher Education provided further financial support for the project. They also thank the German Academic Exchange Service (DAAD) for funding the Yaoundé-Bielefeld Graduate School of Natural Products with Antiparasite and Antibacterial Activities (YaBiNaPA, project number 57316173).

Abbreviations
UV: Ultra-violet; Vis: Visible; IR: Infra-red; FTIR: Fourier-transform infrared spectroscopy; HRESI-MS: High resolution electrospray ionisation mass spectrometry; 1H NMR: Proton nuclear magnetic resonance; 13C NMR: Carbon nuclear magnetic resonance; HSQC: Heteronuclear single quantum coherence; HMBC: Heteronuclear multiple bond correlation;

COSY: Correlation spectroscopy; XRD: X-ray diffraction; DFT: Density functional theory; LCAO: Linear combinations of atomic orbitals; FMO: Frontier molecular orbitals; HOMO: Highest occupied molecular orbital; LUMO: Lowest unoccupied molecular orbital; MEP: Molecular electrostatic potential; PDB: Protein Data Bank; MOE: Molecular Operating Environment; RMSD: Root-mean-square deviation; °C: Degree centigrade; h: Hour; g: Gram; mg: Milligram; L: Liter; mL: Milliliter; µL: Microliter; µg: Microgram; ppm: Parts per million; eV: Electronvolt; Rf: Retention factor; TLC: Thin-layer chromatography; DMSO: Dimethylsulfoxide; MHB: Mueller-Hinton broth; MHA: Mueller-Hinton agar; CLSI: Clinical and Laboratory Standards Institute; ATCC: American Type Culture Collection; MIC: Minimum Inhibitory Concentration; MBC: Minimum Bactericidal Concentration; LMCT: Ligand-to-metal charge transfer;

1. World Health Organization. Global antimicrobial resistance and use surveillance system (GLASS) report 2025. Geneva: World Health Organization; 2025.

2. Murray CJL, et al. Global burden of bacterial antimicrobial resistance 1990–2021: a systematic analysis with forecasts to 2050. Lancet. 2024.

3. Barr J, Sumrra SH, Fatima M, et al. Bridging the gap between theory and treatment: Transition metal complexes as successful candidates in medicine. Coord Chem Rev. 2025;524:216272.

4. Talib AB, Abdulhadi SL. A review of the synthesis and application of azo dyes and metal complexes for emerging antimicrobial therapies. J Chem Rev. 2024;6:94–114.

5. Ren X, Zhang M, Liu J. Recent developments on coumarin hybrids as antimicrobial agents. Pharmaceuticals. 2025;18:1028.

6. Sopbué FE, et al. Synthesis and biological activities of new azo dyes from 3-aminothieno[3,4-c]benzopyran-4-one. Arkivoc. 2016:188–204.

7. Djeukoua DKS, Sopbué FE, Tamokou JD, et al. Synthesis, characterization, antimicrobial activities and electrochemical behavior of new phenolic azo dyes from two thienocoumarin amines. Arkivoc. 2019;6:416–430.

8. Tweedy BG. Plant extracts with metal ions as potential antimicrobial agents. Phytopathology. 1964;55:910–914.

9. Fondjo ES, Feuze SS, Tamokou JD, Tsopmo A, Doungmo G, Wilhelm PSF, Tsamo DLF, Ndjakou BL, Kuiate JR, et al. Synthesis, characterization, and antibacterial activity studies of two Co(II) complexes

with 2-[(E)-(3-acetyl-4-hydroxyphenyl)diazenyl]-4-(2-hydroxyphenyl)thiophene-3-carboxylic acid as a ligand. BMC Chem. 2024;18:75.

10. Sopbué EF, Dennue RK, Tamokou JD, Tsopmo A, Doungmo G, Simon PFW, Lenta BN, Kuiate JR. Synthesis, characterization and in-vitro antibacterial property of Cu(II), Co(II) and Bi(III) complexes with (Z)-1-(2-phenylhydrazono)naphthalen-2(1H)-one as a ligand. Am J Chem. 2023;13(3):83–95.

11. Al-Mousawi SM, El-Apasery MA. Synthesis of some monoazo disperse dyes derived from aminothienochromene. Molecules. 2013;18:8837–8844.

12. Ousmane M, et al. UV-Visible characterization of heterocyclic azo dye derivatives. J Coord Chem. 2007.

13. Kemvou ST, Sopbué EF, Kuiate JR, et al. Synthesis and characterization of azo-based ligands and their metal complexes: antibacterial properties. J Chem Sci. 2020;132:45.

14. Mahendra KT, Alice B, Dahryn T, Gopal N, Khemraj B, Snehasis J. Impact of biofield treatment on spectroscopic and physicochemical properties of p-nitroaniline. Insights Anal Electrochem. 2015;1:1–2.

15. Ömer T. A unique manganese(II) complex of 4-methoxy-pyridine-2-carboxylate: synthesis, crystal structure, FT-IR and UV-Vis spectra and DFT calculations. J Mol Struct. 2017;1144:370–378.

16. Mohammed KB, Tahir MIM, Karen AC, Teng JK. Synthesis, characterization, and bioactivity of Schiff bases and their Cd2+, Zn2+, Cu2+, and Ni2+ complexes. Bioinorg Chem Appl. 2013;2013:362513.

17. Halli MB, Vijayalaxmi PB. Synthesis, spectra characterization and DNA cleavage studies of Co(II), Ni(II), Cu(II), Cd(II), and Hg(II) complexes with benzofuran-2-carbohydrazide Schiff bases. Indian J Chem. 2011;50A:664–669.

18. Nakamoto K. Infrared and Raman Spectra of Inorganic and Coordination Compounds, Part B. 6th ed. Hoboken: Wiley; 2009.

19. Lazaar M, Ben Amor F, Saâd A. Jahn-Teller distortion in octahedral Fe(II) complexes with asymmetric bidentate ligands: a DFT analysis. J Mol Struct. 2025;1322:140115.

20. Parr RG, Pearson RG. Absolute hardness: companion parameter to absolute electronegativity. J Am Chem Soc. 1983;105(26):7512–7516.

21. Geerlings P, De Proft F, Langenaeker W. Conceptual density functional theory. Chem Rev. 2003;103(5):1793–1874.

22. Ayare NN, Ramugade SH, Sekar N. Photostable coumarin containing azo dyes with multifunctional property. Dyes Pigm. 2019;163:692–699 (available online December 2018).

23. Narita T, Hino S, Kawamoto K. Global vs. local reactivity descriptors in predicting antibacterial activity of metal–azo complexes. J Phys Chem B. 2025;129(8):2234–2245.

24. Amin B, Moussa Z, Hassan A. Reactivity descriptors versus biological activity: a cautionary tale for azo-metal complexes. New J Chem. 2025;49(3):1012–1025.

25. Tamokou JD, Tene M, Kuiate JR, Choudhary MI, Tane P. Antifungal and antibacterial activities of methanol extract and compounds from stems of Dissotis thollonii Cogn. J Ethnopharmacol. 2009;124(3):571–577.

26. Agrawal A, Sharma V, Mehta S. Metalloantibiotics: synergistic potential of metal complexes against drug-resistant Staphylococcus aureus. J Inorg Biochem. 2025;254:112521.

27. Chohan ZH, Sumrra SH, Youssoufi MH, Hadda TB. Metal based biologically active compounds: design, synthesis, and antibacterial/antifungal/cytotoxic properties of triazole-derived Schiff bases and their complexes. Eur J Med Chem. 2010;45(7):2739–2747.

28. Vigna J, Marchesi M, Djinni I, Cajnko MM, Sepčić K, Defant A, Mancini I. Indolizinoquinolinedione metal complexes: structural characterization, in vitro antibacterial, and in silico studies. Molecules. 2026;31(2):348.

29. Tripathy SR, Panda PK, Mohapatra RK. Synthesis, characterization, biological and computational insights of some binuclear azo dye-based metal complexes. Appl Organomet Chem. 2025.

30. Ramadan AM, El-Saied FA, Hassan MM. Synthesis, spectroscopic characterization, and in silico antibacterial activity of Mn(II), Co(II), and Fe(III) complexes derived from heterocyclic Schiff bases. Appl Organomet Chem. 2024;38(4):e7312.

31. Morris GM, Lim-Wilby M. Molecular docking. Methods Mol Biol. 2008;443:365–382.

32. Torres PHM, Sodero ACR, Jofily P, Silva-Jr FP. Key topics in molecular docking for drug design. Int J Mol Sci. 2019;20(18):4574.

33. Aldred KJ, Kerns RJ, Osheroff N. Mechanism of quinolone action and resistance. Biochemistry. 2014;53(10):1565–1574.

34. Lionta E, Spyrou G, Vassilatis DK, Cournia Z. Structure-based virtual screening for drug discovery: principles, applications and recent advances. Curr Top Med Chem. 2014;14(16):1923–1938.

35. Okafor SN, Obiahu J, Ezenyilimba C. Recent advances in metal complex antibiotics: mechanisms, activity spectra, and prospects. RSC Med Chem. 2025;16(2):310–328.

36. Imberty A, Hardman KD, Carver JP, Pérez S. Molecular modelling of protein-carbohydrate interactions. Docking of monosaccharides in the binding site of concanavalin A. Glycobiology. 1991;1(6):631–6

Supplementary Files

This is a list of supplementary files associated with this preprint. Click to download.

- 3BMCCSUBMISSIONSMProf.SOPBUEFONDJOSEPTEMBER2026.docx